THE JOURNAL OF PHYSICAL CHEMISTRY B

Article

On the Lorentz Local Electric Field in Soft-Matter Systems

P. Tan, W. J. Tian, L. W. Zhou, and J. P. Huang

J. Phys. Chem. B, **2009**, 113 (16), 5412-5417• DOI: 10.1021/jp8102035 • Publication Date (Web): 30 March 2009

On the Lorentz Local Electric Field in Soft-Matter Systems

P. Tan, W. J. Tian, L. W. Zhou,* and J. P. Huang*

Department of Physics and Surface Physics Laboratory (National Key Laboratory), Fudan University, Shanghai 200433, China

Received: November 20, 2008; Revised Manuscript Received: February 11, 2009

In electric-field-responsive soft-matter systems, the suspended particles respond to the Lorentz local field (LLF), yielding abundant important phenomena. Even though the particles can easily rotate, the LLF was conventionally adopted as a quantity that is independent of rotations in the literature. In contrast, here we design an experiment to measure the LLF between two metallic spheres, one of which is rotating, and report a rotation-driven reduction. Excellent agreement between our experiment and theory reveals the role of the relaxation of dipole moments. Its relevance to biophysics, colloidal physics, and nonlinear physics is also discussed.

I. Introduction

There exist many electric-field-responsive soft-matter systems, e.g., suspensions of colloidal particles or biological cells. In such systems, the suspended particles respond to the Lorentz local field (LLF, namely, the local electric field in the vicinity of a particle), yielding abundant phenomena like electrorotation,[1] the Quincke rotation,[1,2] and shear thinning[3−5] or thickening.[6] It is known that such particles can easily rotate due to a rotating electric field (for electrorotation), a dc electric field (for the Quincke rotation), or a shear flow (for shear thinning or thickening). In dealing with such phenomena, in the literature the LLF was generally calculated by solving the Maxwell equations and the corresponding constitutive relations under appropriate boundary conditions (or, e.g., by using the excluded volume approach[7,8] or a volume average approach based on effective medium theories[9,10]). The process just followed the case in solid-state systems. That is, the particles were simply seen to be stationary no matter whether they are actually rotational or not. Now we are in a position to ask the following question: Do such rotations affect the LLF? Our answer is "yes", which seems to be in sharp contrast to what has been conventionally adopted in the literature. However, until this work, no one has directly revealed the rotation-driven reduction of the LLF in electric-field-responsive soft-matter systems. Thus, in the literature, the LLF was commonly solved by seeing the suspended particle to be stationary. Apparently this should be corrected or revisited according to this work.

Unfortunately, it is very difficult to experimentally measure the LLF in such soft matter systems. We noticed that Tao and Lan[11] conducted an elegant pioneering experiment to measure the interparticle force between a rotating metallic sphere and a stationary one in argon gas and reported that the force can be reduced due to rotations. Their experiment actually implies the reduction of the LLF. Nevertheless, a direct experimental demonstration is lacking, and a theoretical analysis is also in need. This is just the aim of this work. As a model demonstration, following Tao and Lan, we shall specifically design an experiment on two metallic spheres suspended in silicone oil. Then, we are allowed to detect the LLF between a rotating sphere and a stationary one according to the electro-optic Pockels effect[12−14] and the computerized tomography principle.[15,16] Our revealed rotation-driven reduction of a LLF has significant consequences to electric-field-responsive soft-matter systems. For instance, it brings corrections to the reconstruction or revisit of the fundamental theories for electrorotation of biological cells due to a rotating electric field (which is related to nonlinear responses of an electric torque to a LLF in biophysics), for the Quincke rotation due to a dc electric field (which is related to a LLF-threshold phenomena in colloidal physics), and for nonlinear harmonics in suspensions in a shear flow (which is related to nonlinear responses of harmonics to a LLF in nonlinear physics).

The remainder of this paper is organized as follows. In section II, we design an experimental setup to measure the LLF between two metallic spheres: one is rotating, the other is stationary. In section III, we present the experimental results as well as the theoretical analysis. In section IV, we discuss the possible influence of this work. This paper ends with a conclusion in section V.

II. Experimental Section

According to the experimental setup shown in Figure 1, we shall measure only the LLF E_L at the midpoint P, which is located within a $LiNbO_3$ (LN) crystal between the two centers of the two metallic spheres, see Figure 2. In general, the dynamic LLF distribution in the midplane between the two centers of the two spheres can be measured according to the electro-optic Pockels effect[12−14] and the computerized tomography principle.[15,16] The electro-optic Pockels effect produces birefringence in an optical medium subjected to a constant (or varying) electric field E_0, yielding $n_{||} - n_{\perp} \propto E_0$. Here $n_{||}$ (or $n_{\perp}$) indicates the refractive index of the medium, which is measured for a light polarized parallelly (or perpendicularly) to E_0.

In our experiment, we used a LN crystal,[13,14] the applied electric field E_0 was directed along the X axis, and an incident laser beam (linearly polarized along the Y axis) with intensity I_0 was set to propagate along the Z axis, see Figure 1. The X-directed local electric field E_x within the LN crystal at position r in polar coordinates (r,θ) was measured according to

$$E_x(r) = \frac{1}{2\pi^2 C}\int_0^{\pi}\int_{-\infty}^{+\infty}\frac{\phi'(l)}{r\cos\theta - l}\mathrm{d}l\,\mathrm{d}\theta \qquad (1)$$

Equation 1 allows us to experimentally obtain the electric field distribution along the straight line $L(l,\alpha)$, where l denotes the

* To whom correspondence should be addressed. E-mail: (L.W.Z.) lwzhou@fudan.edu.cn and (J.P.H.) jphuang@fudan.edu.cn.

10.1021/jp8102035 CCC: $40.75
Published on Web 03/30/2009

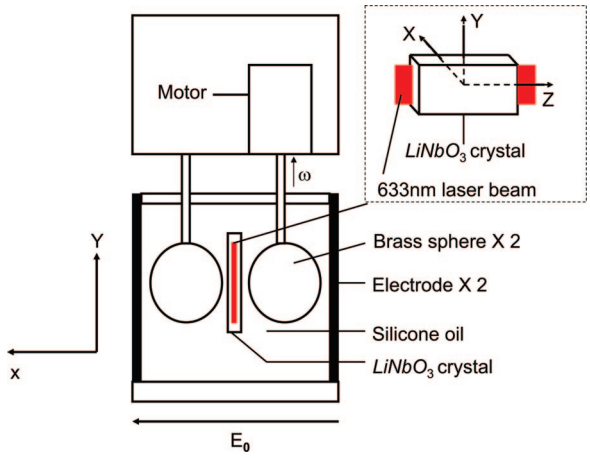

Figure 1. Sketch diagram of the sample cell. The cell has dimensions of 25.258 mm, 25 mm, and 25 mm in the X, Y, and Z directions, respectively, and it is filled with 50 cSt silicone oil. The LN crystal has dimensions of 1 mm, 15 mm, and 30 mm in the X, Y, and Z directions, respectively. The brass sphere on the right is connected with a motor, which causes it to rotate at angular velocity $\omega = \omega\hat{Y}$. For convenience, the velocity ω will be equivalently replaced with rotations per minute, as displayed in Figure 3. Other details can be found in the text.

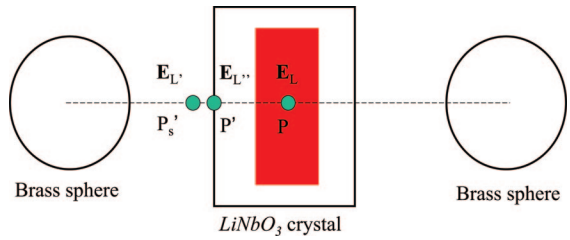

Figure 2. Schematic graph showing the three positions P, P', and P_s' (indicated by three solid circles) and their corresponding local electric fields E_L, $E_{L''}$, and $E_{L'}$. Such notations have been used in eq 2. The sphere on the right is rotating.

vertical distance between the origin of the coordinate (which is taken to be at the midpoint P) and the path L and α the angle between L and the polar coordinate axis. In addition, $C = 2\pi n_0^3\gamma_{22}/\lambda$ and $\phi'(l) = I'(l)/\sqrt{I(I_0-I)}$. For the LN crystal, $n_0 = 2.286$ and $\gamma_{22} = 3.4 \times 10^{-12}$ m/V. $I'(l)$ denotes the derivative of the transmission light intensity I distribution along the Y direction with respect to l, which can be obtained according to our CCD measurement. In addition, the wavelength of the incident laser used in our experiment is $\lambda = 633$ nm. Equation 1 will be used to experimentally measure the LLF, which is displayed in Figure 3a.

In our experiment, we measured only the X-directed LLF at P in order to show the effect of rotations. A dc electric field is applied on the sample cell, which is placed and fixed on an optical platform. The position of the cell can be adjusted mechanically. Two brass spheres with diameter = 12 mm were kept at the same height in the cell. One sphere was connected to a motor, while the other was kept stationary. The rotating axis of the former sphere was Y directed (Figure 1). The surface-to-surface distance between the two spheres is 1.2 mm. The LN crystal in use has dimensions of 1 mm, 15 mm, and 30 mm in the X, Y, and Z directions, respectively, see Figure 1. The crystal is fixed symmetrically between the two spheres with two gaps of 0.1 mm (For instance, the left gap is the distance between the left surface of the LN crystal and the surface of the sphere on the left). The surface-to-surface separation between an electrode and the adjacent sphere is about 0.029 mm. Silicone

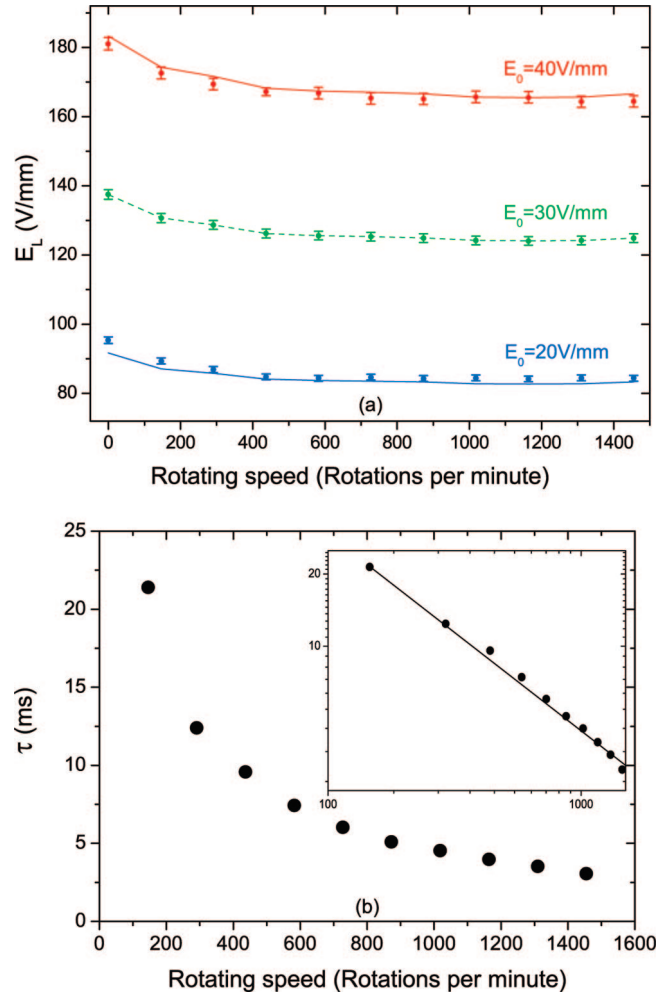

Figure 3. (a) Experimental data (symbols) and theoretical fitting (lines) of the LLF E_L at the center P between the two metallic spheres as a function of the rotating speed of one sphere for different applied dc electric fields E_0. The experimental data of $E_0 = 30$ V/mm is used to extract the relaxation times τ [as depicted in part b], and the other two solid lines for $E_0 = 20$ V/mm and $E_0 = 40$ V/mm are corresponding theoretical results by using the obtained relaxation times. (b) Relaxation times τ's extracted from the experimental data of $E_0 = 30$ V/mm in a by comparing with our theory. The logarithmic scale of τ versus rotating speeds is displayed in the inset, which approximately displays a power-law relation. The straight line in the inset is a guide for the eye.

oil of 50 cSt is sealed in the cell. Care was taken to remove any air bubbles from silicone oil by using a kind of silicone oil with low viscosity, in which air molecules were eliminated by an ultrasonic wave.

A 633 nm laser was used as a light source, and two lenses were employed to expand the laser light beam into a homogeneous beam with a diameter of 15 mm. Then, this beam passed through a slit, which is narrower than the LN crystal, see Figure 1. Next, it propagated along the Z axis (see Figure 1) and successively passed through a Y polarizer, the sample cell (Figure 1), and an X polarizer. The outgoing beam was captured by a CCD camera. The changes of the light intensity before and after applying the electric field E_0 were measured, and the phase shift along different paths was calculated.

During the experiment, one problem should be carefully treated in order to warrant the precision. That is, when one sphere is rotating, there exists a hydrodynamic force acting upon the LN crystal, which may yield vibrations of the LN crystal. If so, the laser beam will not be able to propagate along the Z

direction within the LN crystal. To overcome it, we fixed the LN crystal to avoid hydrodynamic pressure and thus the above-mentioned vibrations. The efficiency of doing so was carefully confirmed. When one sphere was rotating without an external field E_0, the transmission light intensity was also equal to that of the static case, which indicated that the hydrodynamic pressure has no evident effect on the LN crystal.

III. Experimental Results and Theoretical Analysis

The LLF E_L experimentally measured at P is displayed in Figure 3a as a function of the rotating speed of one sphere. The external fields E_0 used in the present case is much smaller than the usual values (>1 kV/mm) adopted in field-responsive colloidal suspensions like electrorheological fluids. This is to avoid breakdown of the silicon oil between the two spheres in the model system. The error bar of our measurement in Figure 3a combines those only from the laser intensity (less than 0.25%) and intensity distribution measurement (less than 2.5%). It is found that the LLF E_L decreases with the increasing rotating speed. At lower rotating speed, the reduction of E_L is significant, while at higher rotation speed, the change of E_L is no longer evident. The reduction ratio of E_L, which is defined as the ratio of the E_L difference (between the zero and maximum rotating speed) to the E_L at zero rotating speed, is about 10% for the current experimental setup. This can also be used to qualitatively explain Tao and Lan's experiments[11] in which they reported that the interparticle force between a rotating metallic sphere and a stationary one in argon gas was caused to decrease as the rotating speed increases.

For our system as displayed in Figure 1, the theoretical calculation for the LLF E_L at P can be given by considering the continuity condition of the normal electric displacement at the center P' of the left (or right) surface of the LN crystal

$$E_{L'}\varepsilon_1 = E_{L''}\varepsilon_2 \tag{2}$$

where $E_{L'}$ denotes the local electric field at the position P'_s (which is very close to P') in silicone oil and $E_{L''}$ the corresponding local field at P' in the LN crystal. For clarity, the notations used in eq 2 have been schematically shown in Figure 2. Owing to $\varepsilon_1 \ll \varepsilon_2$ adopted in our experiment (the dielectric constant of silicone oil $\varepsilon_1 = 2.8$, and that of the LN crystal $\varepsilon_2 = 84.6$), the LLF between the centers of the two metallic spheres inside the LN crystal is assumed to be uniformly distributed for the sake of simplification. In fact, the actual inhomogeneity of such LLF in the crystal is within about 1 order of magnitude, as revealed by the finite element analysis. Thus, we are allowed to assume $E_L = E_{L''}$. As above mentioned, here E_L denotes the LLF at the midpoint P. Consequently, eq 2 enables us to compare our experiment and theory. To proceed, the local electric field $E_{L'}$ in eq 2 is determined by

$$E_{L'} = E_0 + (E_\alpha + E_{\alpha 1} + E_{\alpha'} + E_{\alpha 2} - E_{\alpha 0}) + (E_\beta + E_{\beta 1} + E_{\beta'} + E_{\beta 2} - E_{\beta 0}) \tag{3}$$

For this equation, we have only taken into account the following interactions. Details: The interaction between the left static metallic sphere α and the left electrode can be seen as that between the sphere α and its image sphere α_1. By using the multiple image method of dipoles,[18] the multipolar interaction between spheres α and α_1 can be captured, and the total dipole moments in each α or α_1 can be expressed analytically, which yield the electric fields E_α and $E_{\alpha 1}$ at the position P'_s, respectively. In the mean time, the interaction between the sphere α and the LN crystal can also be seen as that between the sphere α and its image sphere α_2. Similarly, the multiple image method of dipoles helps in determining the total dipole moment in α or α_2, which yields $E_{\alpha'}$ and $E_{\alpha 2}$ at P'_s, respectively. In eq 3, $E_{\alpha 0}$ denotes the electric field at P'_s produced by the dipole moment of the single static sphere α in the presence of E_0. On the same footing, E_β, $E_{\beta 1}$, $E_{\beta'}$, $E_{\beta 2}$, and $E_{\beta 0}$ in eq 3 arise from the rotating metallic sphere β on the right.

The multiple image method of dipoles for two unequal spheres[17,18] can be generally performed to solve each of the following four pairs of electric fields: E_α and $E_{\alpha 1}$, $E_{\alpha'}$ and $E_{\alpha 2}$, E_β and $E_{\beta 1}$, and $E_{\beta'}$ and $E_{\beta 2}$, respectively. Therefore, in the following, let us consider two general unequal metallic spheres, A and B, with radius a and b, respectively. Then we apply a uniform electric field to the system. This induces a dipole moment into each of the spheres. The dipole moments of spheres A and B are given by p_{A1} and p_{B1}, respectively. Next, we include the image effects. The dipole p_{A1} induces an image dipole p_{A2} into sphere B, while p_{A2} induces another image dipole in sphere A. As a result, multiple images are formed. Similarly, p_{B1} induces an image p_{B2} into sphere A. The formation of multiple images leads to an infinite series of image dipoles. The sum of the dipole moments inside each sphere is first calculated according to eqs 38−41 of ref 18 and then used to produce the local field at P'_s.

To better understand the underlying physics, below we briefly review the formulas derived from the multiple image method of dipoles for two unequal spheres A and B. We use r_0 to denote the center-to-center distance between the two spheres A and B. The original dipole moments parallel with the line joining the centers of the two spheres (longitudinal case) are $p_{1,A}$ [eq 15] for sphere A and $p_{1,B}$ [eq 15] for sphere B. Then, the local field at P'_s contributed by the sum of the longitudinal dipole moments in spheres A and B[17,18] can be, respectively, given by

$$E_A^L(R) = \frac{1}{4\pi\varepsilon_1}\left(\sum_{n=1}^{\infty}\frac{2p_{n,A}^L}{(R/2 - x_{n,A})^3} + \sum_{n=1}^{\infty}\frac{q_{n,A}^L}{}\right.$$

Here R (or R') denotes the distance between the center of sphere A (or B) and P'_s. Since an infinite series of image dipole moments is formed in sphere A, the nth-order result $p_{n,A}^L$ is given in odd-order ($p_{n,A}^o$) and even-order ($p_{n,A}^e$) terms as

$$p^{e}_{n,A} = p_{1,B}\left(\frac{a \sinh 2\vartheta}{r_0 \sinh n\vartheta}\right)^3 \quad (7)$$

where the superscript 'o' denotes odd-order terms and 'e' even-order terms. Here, ϑ is defined as $\cosh 2\vartheta = (r_0^2 - a^2 - b^2)/2ab$. Both $p_{1,A}$ and $p_{1,B}$ are given by eq 15 below. Similarly, $x_{n,A}$ (the position of the nth-order image dipole moment $p^{L}_{n,A}$ and image charge $q^{L}_{n,A}$) can be expressed as

$$x^{o}_{n,A} = \frac{ar_0 \sinh(n-1)\vartheta}{a \sinh(n-1)\vartheta + b \sinh(n+1)\vartheta} \quad (8)$$

$$x^{e}_{n,A} = \frac{a^2 \sinh n\vartheta + ab \sinh(n-2)\vartheta}{r_0 \sinh n\vartheta} \quad (9)$$

And $q^{L}_{n,A}$ admits

$$q^{o}_{n,A} = \frac{p_{1,A}}{a}\frac{br_0 \sinh 2\vartheta \sinh(n-1)\vartheta}{(a \sinh(n-1)\vartheta + b \sinh(n+1)\vartheta)^2} \quad (10)$$

$$q^{e}_{n,A} = \frac{p_{1,B}}{b}\frac{a \sinh 2\vartheta(a \sinh(n-2)\vartheta + b \sinh n\vartheta)}{(r_0 \sinh n\vartheta)^2} \quad (11)$$

In addition, since the two spheres are isolated, two charges q^{L}_{cA} and q^{L}_{cB}[17,18] should be put at the centers of the spheres A and B, respectively, in order to keep charge neutralization. Here, q^{L}_{cA} is given by

$$q^{L}_{cA} = \frac{\sum_{n=1}^{\infty} q^{L}_{n,B} \sum_{n=2}^{\infty} \lambda^{e}_{n,A} - \sum_{n=1}^{\infty} q^{L}_{n,A} \sum_{n=1}^{\infty} \lambda^{o}_{n,B}}{\sum_{n=2}^{\infty} \lambda^{e}_{n,A} \sum_{n=2}^{\infty} \lambda^{e}_{n,iB} - \sum_{n=1}^{\infty} \lambda^{o}_{n,A} \sum_{n=1}^{\infty} \lambda^{o}_{n,B}} \quad (12)$$

Further, the two point charges q^{L}_{cA} and q^{L}_{cB} also induce a series of image charges, whose normalized magnitudes in sphere A, $\lambda^{o}_{n,A}$ and $\lambda^{e}_{n,A}$ can be found in refs 17 and 18 are, respectively, represented as

$$\lambda^{o}_{n,A} = \frac{b \sinh 2\vartheta}{a \sinh(n-1)\vartheta + b \sinh(n+1)\vartheta} \quad (13)$$

$$\lambda^{e}_{n,A} = \frac{a \sinh 2\vartheta}{r_0 \sinh n\vartheta} \quad (14)$$

Here, $\lambda^{o}_{n,A}$ (or $\lambda^{e}_{n,iA}$) was normalized to q^{L}_{cA} (or q^{L}_{cB}).

If the sphere is rotating, the X-directed component of the first-order dipole moment is given by[19]

$$p_1 = \frac{p^{(0)}}{1 + (\omega\tau)^2} \quad (15)$$

where $p^{(0)} = 4\pi\varepsilon_2 a^3 E_0$ (or $p^{(0)} = 4\pi\varepsilon_2 b^3 E_0$) for the static metallic sphere A (or B). p_1 in eq 15 just represents $p_{1,A}$ (or $p_{1,B}$) of rotating sphere A (or B) with angular velocity ω. The physical meaning of eq 15 is as follows: The dipole moment of a sphere is constant, $p_1 = p^{(0)}$, as the sphere is stationary ($\omega = 0$). Momentarily at the rotated position, the displaced dipole moment deviates from the static one $p^{(0)}$. The distribution will tend to relax to a nonstatic equilibrium distribution p_1 at a certain rate $1/\tau$, depending on the relaxation time τ, which is related to the material, geometry, and rotating speed of the spheres.[20] Thus far there is no first-principles approach for deriving τ for the case of our interest. In this work, the τ will be determined by comparing our theory with the experimental data (see Figure 3b). Equation 15 is actually a steady-state solution,[19] which means that p_1 should only be achieved after a time period, which is long enough to ensure the steady-state dipole-moment distribution at nonstatic equilibrium. In addition, eq 15 shows that the product of $\omega\tau$ plays a key role in the magnitude of p_1. As $\omega\tau$ increases, p_1 deviates from $p^{(0)}$ more significantly. As $\omega\tau$ tends to zero (the static case), p_1 reduces to $p^{(0)}$, as expected.

Similar to the expressions for $p^{L}_{n,A}$ [eqs 6 and 7], $x_{n,A}$ [eqs 8 and 9], $q^{L}_{n,A}$ [eqs 10 and 11], q^{L}_{cA} [eq 12], $\lambda^{o}_{n,A}$ [eq 13], and $\lambda^{e}_{n,A}$ [eq 14], we are allowed to readily express $p^{L}_{n,B}$, $x_{n,B}$, $q^{L}_{n,B}$, q^{L}_{cB}, $\lambda^{o}_{n,B}$, and $\lambda^{e}_{n,B}$ in eqs 4 and 5 as long as we exchange $A \leftrightarrow B$ and $a \leftrightarrow b$, respectively.

Now we are in a position to present our theoretical results. In Figure 3a, the dashed line (corresponding to $E_0 = 30$ V/mm) is used to extract the fitting relaxation times τ's [which are displayed in Figure 3b], and the solid lines are theoretical calculations based on the extracted relaxation times. In other words, for obtaining the solid lines, only E_0 is tunable while keeping all other parameters unchanged. The theoretical result fits very well with the experimental data, which indicates that the relaxation time of the system varies little with the magnitude of E_0. In addition, Figure 3b shows that the relaxation times in use decreases greatly with the increasing rotating speed. The relation between them is approximately power law, exhibiting the possible property of scale invariance (within the range of rotating speeds). Owing to the above analysis and eq 15, we can safely conclude that the LLF's reduction is due to the rotation-driven relaxation of the dipole moment. However, the contributions to the dipole moment are composed of two origins: one is from the brass sphere itself; the other is from the air and water molecules[27] adsorbed onto the surface of the spheres. Nevertheless, we note that the relaxation times shown in Figure 3b are $\sim 10^{-3}$ s. In addition, the actual relaxation time of charges (or dipole moments) in brass spheres is small enough to be neglected. Thus, we conclude that the relaxation is due to the dipolar molecules adsorbed to the spheres. That is, if there is an external electric field, the dipolar molecules prefer to stay at the two ends of the spheres where the local field is maximal, and they reach nonstatic equilibrium once the sphere is rotating. Actually, if we use the brass spheres without air or water molecules adsorbed, the measured LLF at P cannot be changed at all with respect to the rotating speed of one sphere. [As tiny air and water molecules are adsorbed onto the spheres, the expression for $p^{(0)}$ is reasonably assumed to be the same as that for a pure metallic sphere, as already adopted in eq 15. In other words, all the above equations for the multiple image method of dipoles in metallic spheres without adsorbed molecules remain approximately valid for the spheres with adsorbed molecules. This approximation can be justified by using the effective moment method.[1]] The consideration may be readily extended to the case of rotating dielectric particles, in which charges can be induced to appear at the two ends of the particle and further reach nonstatic equilibrium as the particle is rotating. The relaxation time for the polarization charges (or dipole moment) in dielectric spheres is just $\sim 10^{-3}$ s.[28,29] Therefore, the revealed mechanism for the rotation-driven reduction of

LLFs qualitatively holds for various kinds of particles in real suspensions, like biological cells.

IV. Discussion

We experimentally investigated two metallic spheres and observed rotation-driven reduction of the LLF. Good agreement between our experiment and theory helped to reveal the underlying physical mechanism: The reduction originates from dipole-moment redistribution for reaching nonstatic equilibrium. We found that the rotation could lead to about 10% reduction of the LLF for the model system. Specifically, at a rotating speed of 291 rotations/min or 4.85 rotations/s, the reduction ratio of the LLF could, respectively, be 6.46% for $E_0 = 40$ V/mm, 6.4% for $E_0 = 30$ V/mm, and 8.9% for $E_0 = 20$ V/mm. It is worth noting that such a rotating speed is reachable in many field-responsive soft-matter systems. Besides linear responses, nonlinear responses to the LLF may also play an important role in various aspects, which thus makes our achievement significant in several fields. In general, this work brings three possible corrections in biophysics, colloidal physics, and nonlinear physics.

1. First Correction in the Field of Biophysics: The Fundamental Theory for Electrorotation Due to a Rotating Electric Field Is Being Corrected. Electrorotation is a phenomenon in which an interaction between a rotating electric field and suspended dielectric particles leads to a rotational motion of the particles. Electrorotation has been increasingly employed as a sensitive tool for noninvasive studies of a broad variety of microparticles, ranging from living cells to spores, seeds, synthetic materials, as well as nanowires, see, e.g., refs 1, 22, and 23.

According to the known fundamental theory for electrorotation, the rotating speed of a cell is given by the steady-state equilibrium condition defined by a balance of the electric torque Γ^e and the viscous retarding torque Γ^η, $\Gamma^e + \Gamma^\eta = 0$,[1] where Γ^e is expressed as the cross product between the induced electric dipolar moment and the LLF. (Here we only take the "dipolar moment" as an example. In a real situation, "multipolar moments" also play a role as long as the cells are close to each other.) Thus, Γ^e is proportional to the LLF magnitude squared, which was commonly determined by seeing the cell to be stationary in the literature. However, the rotating speed, e.g., 4.85 rotations/s or even much higher, is easily realizable for a cell with respect to an external rotating electric field (since this rotation is not always synchronous). In this case, the influence of our reported rotation-driven reduction of the LLF should be taken into account carefully because it is no longer neglectable due to the nonlinear response to the LLF. In this regard, the underlying fundamental theory for describing electrorotation should be reconstructed or revisited by including our new achievement. For this purpose, more theoretical and experimental work is needed.

2. Second Correction in the Field of Colloidal Physics: The Fundamental Theory for the Quincke Rotation Due to a dc Electric Field Is Being Corrected. The Quincke rotation is a spontaneous rotation exhibited by small insulating particles suspended in conductive liquid when subjected to a dc electric field exceeding a certain threshold value. In the case of the Quincke rotation, the rotating speed, e.g., 4.85 rotations/s or much higher, can be easily reached. According to the dynamic equation of motion, its rotating speed Ω is well known to be determined by[1,2]

$$\Omega = \pm\tau_{MW}^{-1}\sqrt{\frac{E_{LLF}^2}{E_c^2} - 1} \tag{16}$$

where τ_{MW} is the Maxwell−Wagner relaxation time. Our revealed rotation-driven reduction of the LLF can bring nontrivial physics to the Quincke rotation, especially at the LLF E_{LLF} close to the critical field E_c. For instance, when E_{LLF} (which was commonly obtained by seeing the particle to be stationary in the literature) is larger than E_c, the particle begins to rotate according to the above equation. However, after the particle rotates, our revealed phenomenon can yield decreasing E_{LLF}, which will cause the particle to slow (or even stop) again according to eq 16. On the other hand, once the particle slows indeed, the resulting E_{LLF} increases and makes the particle rotate the same as before according to eq 16. Thus, an oscillating behavior is likely to appear. In this case, based on eq 16, new fundamental theory for the possible nontrivial oscillating behavior should be established by including the influence of rotation-driven reduction of the LLF. In this direction, much theoretical and experimental work is also expected.

3. Third Correction in the Field of Nonlinear Physics: The Fundamental Theory for Nonlinear Harmonics Is Being Corrected. In general, the rotating speed, e.g., 4.85 rotations/s or much higher, is easily realizable for a particle in suspensions in a shear flow. When a suspension consisting of dielectric particles having nonlinear characteristics is subjected to a sinusoidal electric field, the electric response will in general consist of ac fields at frequencies of the higher-order harmonics. By measuring the nonlinear ac responses of rotating particles, it is possible to determine the relaxation time and rotational speed of the particles.[24] For instance, for a single spherically symmetrical dielectric particle, its dipole moment p can be expressed in terms of harmonics such that[25,26]

$$p = p_\omega \sin \omega t + p_{3\omega} \sin 3\omega t + p_{5\omega} \sin 5\omega t + \cdots \tag{17}$$

Here the harmonics of the induced dipole moments can be given by

$$p_\omega = h_1 E_{LLF} + \frac{3}{4} h_3 \chi_1 E_{LLF}^3 + \frac{5}{8} h_5 \chi_1^2 E_{LLF}^5 \tag{18}$$

$$p_{3\omega} = -\frac{1}{4} h_3 \chi_1 E_{LLF}^3 - \frac{5}{16} h_5 \chi_1^2 E_{LLF}^5 \tag{19}$$

$$p_{5\omega} = \frac{1}{16} \chi_1^2 E_{LLF}^5 \tag{20}$$

where h_1, h_3, and h_5 are quantities related to material properties[26] and χ_1 is the third-order nonlinear dielectric susceptibility. Evidently, such harmonics are strongly related to the LLF nonlinearly. Clearly, the rotation-driven reduction of the LLF could lead to a significant impact on the corresponding harmonics, especially on the higher-order harmonics. For instance, if the reduction ratio for LLF is 6.5%, the reduction ratio for $p_{5\omega}$ will become as high as 32.5% according to eq 20. Apparently, in view of the nonlinear responses to the LLF, it is quite necessary to reestablish or revisit the fundamental theory by including our new achievement.

Our experiment has shown that relaxation times are dependent on rotating speed. It is physical and reasonable in view of dirty

particles and the mobility of molecules (or ions) adsorbed on the surface of the spheres. In other words, once the metallic spheres are clean or there are no molecules (or ions) adsorbed, the corresponding relaxation time should be fixed for the current parameter set no matter whether the spheres are rotating or not.

Besides the image method used in this work, some other theories like the Rayleigh method[30,31] and a multipole-expansion theory[32,33] can be more accurately adopted to treat the present system from the quantitative point of view. On the other hand, from the qualitative point of view, comparing with such methods, the image method works the same, and it is somehow easy to use due to its compact framework.

Depending on different situations, various types of rotations can exist in soft-matter systems, like uniform rotations, rotations in oscillations, and so on. In this work, we focused on the case of uniform rotations only. Here we should claim that the effects on relaxation times should be different for the case of rotations in oscillations, due to the different dynamic effects of the molecules (or ions) adsorbed

In addition, the electric relaxation process of many rotating particles can also be coupled with each other.[34] For such systems, besides the additional many-body coupling effects, multipolar interactions should also play an important role, as revealed in this work.

V. Conclusion

Until this work, no one has directly revealed the rotation-driven reduction of the LLF in electric-field-responsive soft-matter systems. Thus, in the literature, the LLF was commonly solved by seeing the suspended particle to be stationary. This should be corrected, or at least revisited carefully, according to this work because we convincingly demonstrated the rotation-driven reduction of the LLF. This reduction arises from the relaxation of dipole moments, as revealed by the good comparison between our experiment and theory. Our work further brings possible (slight) corrections to some fundamental theories in biophysics, colloidal physics, and nonlinear physics.

Acknowledgment. We thank Professor P. Sheng and Dr. J. J. Xiao for fruitful discussion. We also acknowledge the financial support by the National Natural Science Foundation of China under Grant Nos. 10334020, 10574027, 10604014, and 10874025, by the Shanghai Education Committee and the Shanghai Education Development Foundation ("Shu Guang" project under Grant No. 05SG01), and by Chinese National Key Basic Research Special Fund under Grant No. 2006CB921706.

References and Notes

(1) Jones, T. B. *Electromechanics of Particles*; Cambridge University Press: New York, 1995.
(2) Cebers, A. *Phys. Rev. Lett.* **2004**, *92*, 034501.
(3) Halsey, T. C. *Science* **1992**, *258*, 761.
(4) Cao, J. G.; Huang, J. P.; Zhou, L. W. *J. Phys. Chem. B* **2006**, *110*, 11635.
(5) Xu, L.; Tian, W. J.; Wu, X. F.; Cao, J. G.; Zhou, L. W.; Huang, J. P.; Gu, G. Q. *J. Mater. Res.* **2008**, *23*, 409.
(6) McWhirter, J. L. *J. Chem. Phys.* **2008**, *128*, 034502.
(7) Landauer, R. Electrical Transport and Optical Properties of Inhomogeneous Media. *AIP Conference Proceedings 40*; Garland, J. C., Tanner D. B., Eds.; AIP: New York, 1978.
(8) Bragg, W. L.; Pippard, A. B. *Acta Crystallogr.* **1953**, *6*, 865.
(9) Levy, O. *Phys. Rev. E* **2003**, *68*, 011407.
(10) Huang, J. P.; Yu, K. W. *Phys. Rep.* **2006**, *431*, 87.
(11) Tao, R.; Lan, Y. C. *Phys. Rev. E* **2005**, *72*, 041508.
(12) Shen, Y.; Watanabe, T.; Arena, D. A.; Kao, C. C.; Murphy, J. B.; Tsang, T. Y.; Wang, X. J.; Carr, G. L. *Phys. Rev. Lett.* **2007**, *99*, 043901.
(13) Garzarella, A.; Qadri, S. B.; Wieting, T. J.; Wu, D. H. *J. Appl. Phys.* **2005**, *97*, 113108.
(14) Garzarella, A.; Qadri, S. B.; Wieting, T. J.; Wu, D. H. *J. Appl. Phys.* **2005**, *98*, 043113.
(15) Galik, K.; Senut, B.; Pickford, M.; Gommery, D.; Treil, J.; Kuperavage, A. J.; Eckhardt, R. B. *Science* **2004**, *305*, 1450.
(16) Jie, H.; Shen, M.; Xu, J.; Chen, W. X.; Jin, Y.; Peng, W. N.; Fu, X. B.; Zhou, L. W. *Appl. Phys. Lett.* **2004**, *85*, 13.
(17) Jiang, Z. *J. Electrostat.* **2003**, *58*, 247.
(18) Ju, Y.; Huang, J. P. *J. Phys. Chem. B* **2008**, *112*, 7865.
(19) Wan, J. T. K.; Yu, K. W.; Gu, G. Q. *Phys. Rev. E* **2001**, *64*, 061501.
(20) Gu, G. Q.; Yu, K. W.; Hui, P. M. *J. Chem. Phys.* **2002**, *116*, 10989.
(21) Arnold, W. M.; Zimmermann, U. *Z. Naturforsch. C* **1982**, *37*, 908.
(22) Becker, F. F.; Wang, X. B.; Huang, Y.; Pethig, R.; Vykoukal, J.; Gascoyne, P. R. *Proc. Natl. Acad. Sci. U.S.A.* **1995**, *92*, 860.
(23) Edwards, B.; Mayer, T. S.; Bhiladvala, R. B. *Nano Lett.* **2006**, *6*, 626.
(24) Tian, W. J.; Huang, J. P.; Yu, K. W. *Phys. Rev. E* **2006**, *73*, 031408.
(25) Huang, J. P.; Wan, J. T. K.; Lo, C. K.; Yu, K. W. *Phys. Rev. E* **2001**, *64*, 061505(R) .
(26) Huang, J. P.; Gao, L.; Yu, K. W. *J. Appl. Phys.* **2003**, *93*, 2871.
(27) In fact, some ions can also contribute. However, owing to their neglectable amount, they should contribute much less than the molecules.
(28) Wen, W.; Ma, H.; Tam, W. Y.; Sheng, P. *Phys. Rev. E* **1997**, *55*, R1294.
(29) Tian, W. J.; Liu, M. K.; Huang, J. P. *Phys. Rev. E* **2007**, *75*, 021401.
(30) Rayleigh, L. *Philos. Mag.* **1892**, *34*, 481.
(31) Gu, G. Q.; Yu, K. W.; Hui, P. M. *Phys. Rev. B* **1998**, *58*, 3057.
(32) Jackson, J. D. *Classical Electrodynamics*, 3rd ed.; John Wiley & Sons, Inc.: New York, 2001.
(33) Clercx, H. J. H.; Bossis, G. *Phys. Rev. E* **1993**, *48*, 2721.
(34) Gu, G. Q.; Yu, K. W. *China Particuol.* **2005**, *3*, 47.

JP8102035